Dual-Gate Fet-Based Charge Sensor Enhanced by In-Situ Electrode Decoration in a MEMS Organs-On-Chip Platform

Aydogmus, Hande; van Ginkel, H. Joost; Galiti, Anna-Danai ; Hu, Michel; Frimat, Jean-Philippe; van den Maagdenberg, Arn ; Zhang, GuoQi; Mastrangeli, Massimo ; Sarro, Pasqualina M.

DUAL-GATE FET-BASED CHARGE SENSOR ENHANCED BY IN-SITU ELECTRODE DECORATION IN A MEMS ORGANS-ON-CHIP PLATFORM

Hande Aydogmus[1], H. Joost van Ginkel[1], Anna-Danai Galiti[1], Michel Hu[2,3], Jean-Philippe Frimat[2,3], Arn van den Maagdenberg[2,3], GuoQi Zhang[1], Massimo Mastrangeli[1], and Pasqualina M. Sarro[1]

[1]ECTM, Department of Microelectronics, Delft University of Technology, the Netherlands.
[2]Department of Human Genetics, Leiden University Medical Centre, the Netherlands.
[3]Department of Neurology, Leiden University Medical Centre, the Netherlands.

ABSTRACT

Continuous monitoring of tissue microphysiology is a key enabling feature of the organ-on-chip (OoC) approach for drug screening and disease modeling. Sensing charged species in OoC tissue microenvironments is thereby essential. However, the inherently small (*i.e.*, cm) size of OoC devices poses the challenging requirement to integrate miniaturized and highly sensitive *in situ* charge sensing components to maximize signal extraction from small volumes (nL to µL range) of media used in these devices. Here we meet this need by presenting a novel dual-gate field-effect transistor-based charge sensor integrated within an optically transparent microelectromechanical (MEM) OoC device. Post-process mask-less decoration of Ti sensing electrodes by spark-ablated Au nanoparticle films significantly increases the effective electrode surface area and thus sensor sensitivity while retaining the CMOS-compatibility of the wafer-level fabrication process. We validate the biocompatibility of the sensor and its selective response to poly-D-lysine and KCl, and provide a perspective on monitoring cultures and differentiation of hiPSC-derived cortical neurons on our OoC device.

KEYWORDS

Biosensor, charge sensing, electrodes, microfabrication, organ-on-chip, spark ablation, neurons

INTRODUCTION

Organs-on-chip (OoCs) are dynamic tissue culture devices which mimic microphysiological environments to recapitulate *in vivo*-like organ functions *in vitro* and thus enhance the efficiency of drug development and disease modelling [1]. Among the key features distinguishing OoCs from established tissue culture technologies, automated monitoring of biological cues, such as charged species, is essential to reduce user intervention and improve system's ease of use and reliability [2]. In this respect, dynamic electric sensing can meet user needs without recurring to terminal optical labeling and microscopy techniques, which deteriorate cells' wellbeing.

To provide compact charge sensing solutions in OoCs, the integration of a floating gate [3-5] field-effect transistor (FG-FET)-based electrochemical sensor within a microelectromechanical OoC device was previously demonstrated [6]. Prior examples of FET-based bio-chemical sensing include tracking metabolic activity of neurons [7-8] and of pH [9]. Our hybrid OoC combines in a single device the benefit of soft polymeric substrates, suitable for tissue culturing under physiologically relevant conditions, with that of extremely compact and inherently signal-amplifying electronic sensing units, uniquely enabled by silicon-based microfabrication [10]. Building on that, in this paper, we
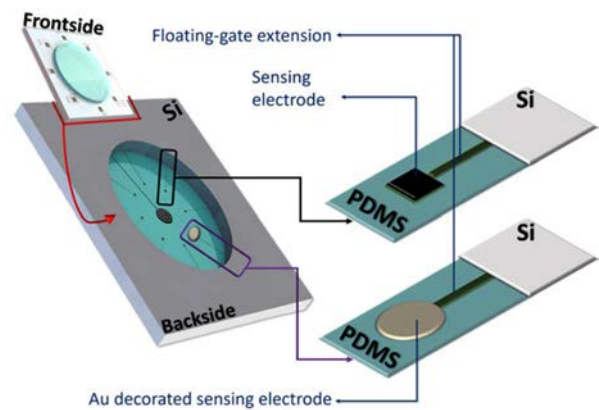

Figure 1: Schematic of the MEM OoC device with integrated FET-based charge sensor. Right insets show sensing electrodes over the suspended membrane without (top) and with (bottom) decoration with Au film.

show significant enhancement in sensitivity and in selective response of the FG-FET-based charge sensor. Both breakthroughs were enabled by the introduction of a novel dual-control-gate configuration and by *in situ* decoration of the sensing electrode surface with nanoporous Au thin films (Fig. 1).

The OoC device is fabricated by means of a mostly CMOS-compatible co-fabrication process. The charge sensor therein replaces the function of an external reference electrode with that of a pair of control gates (CG_1 and CG_2) capacitively coupled to the floating gate. An extension of the FG reaches over the suspended polymer membrane, representing the optically accessible tissue culturing area, and terminates with a sensing electrode. The charge stored in the dielectric layer (silicon oxide) between CG_1 and FG sets the working point of the transistor, whereas the electrolyte bridging CG_2 and FG serves as dielectric as well as solution-under-test (SOT). Biasing CG_2 provides electric field towards the sensing electrode at the tip of the FG extension. This promotes the binding of charged species on the sensing surface and thus provides higher sensitivity (Fig. 2(a)). In turn, the charges in close proximity of the sensing electrode can be continuously detected by monitoring the drain current (I_D) of the transistor.

Charge sensing exploits the electrical double layer [11], as it involves (reversible) binding by charged species in solution to sites available at the sensing surface. Therefore, to further enhance sensitivity we aimed at expanding the effective electrode surface and increasing the number of available binding sites by means of surface structuring with Au. Due to its inherent biocompatibility and inertness, Au has been widely used for biosensing applications as a
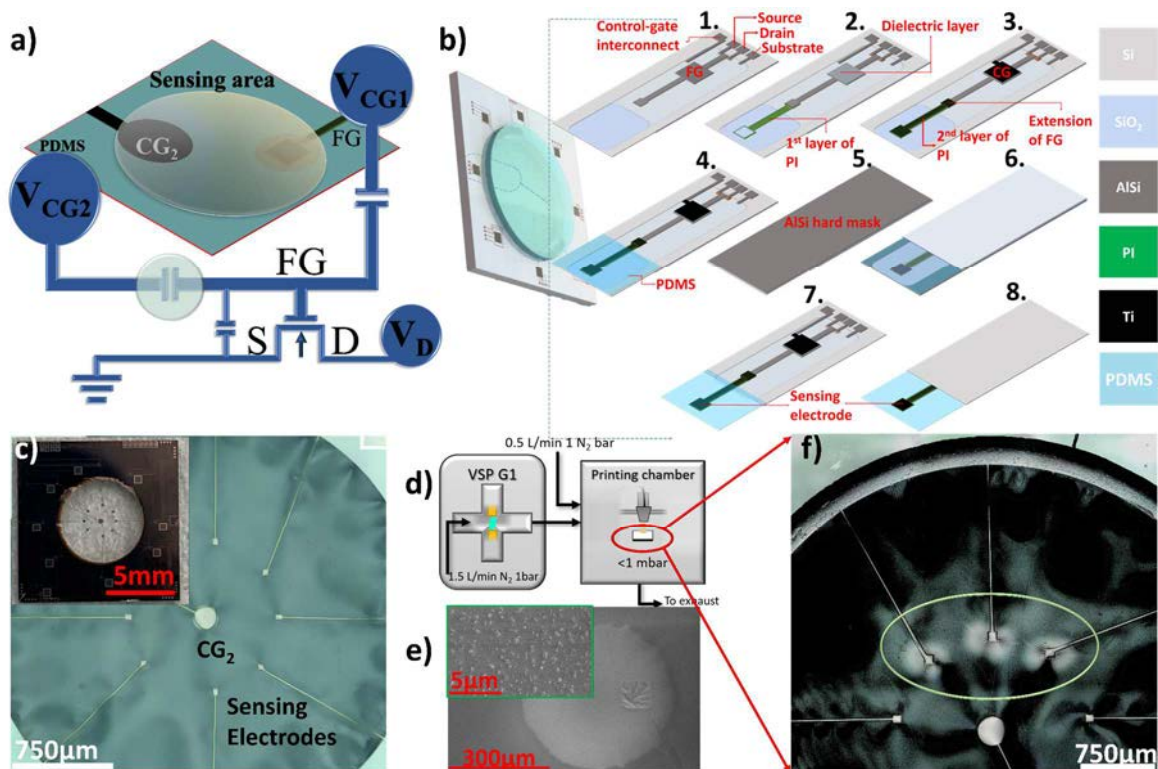
Figure 2: a) Schematic of the sensing mechanism, showing a section of the sensing area with CG$_2$ and FG. The dual-control-gate configuration provides measurement of charges on the floating-gate extensions. b) Wafer-level fabrication of the dual-gate FG-FETs. c) Laser-optical microscope image of the frontside of a single chip. Second control-gate and sensing electrodes are visible. Inset shows the full chip after dicing. d) Sketch of the nanomaterial printer setup. e) SEM micrograph of local decoration of sensing electrodes with Au nanoparticle films (film morphology evidenced in the inset.) f) Backside micrograph of the chip by laser-optical microscopy, showing Au decoration on 3 of the 8 sensing electrodes.

selective material, including monitoring pH and neuronal activity [8], tracking the morphology of cancer cells and fibroblasts [12], and DNA hybridization [13]. However, Au's well-known incompatibility with CMOS process flows imposes its post-processing. Here, nanostructured, microscopically rough Au films were deposited by inertial impaction of a pure Au nanoparticle (NP) aerosol generated by spark ablation. The technique is mask-less (avoiding the issues of conducting lithography over substrates with high topography), spatially-selective, fast, and is conducted at room temperature. Moreover, while it does not presently allow batch wafer post-processing, it does not harm the flexible and suspended polymeric membranes supporting the electrodes, and yields surface roughness figures superior to other more cumbersome post-processing techniques (*e.g.* flow coating), let alone CMOS-compatible ones (*e.g.*, e-beam evaporation, sputtering, atomic layer deposition).

FABRICATION

Fabrication of the FET

A 4-inch, 525 μm-thick, single-side polished p-type Si wafer was used for the fabrication of both nMOS- and pMOS-based sensors using a standard BiCMOS process (Fig. 2(b)). After defining source and drain terminals by ion implantation, a 200 nm-thick gate oxide layer was thermally grown. A 6 μm-thick PECVD oxide layer was deposited and patterned on the wafer backside as etch hard mask. A 1000 nm-thick layer of AlSi was sputtered and

patterned on the front side to implement electrical interconnects and floating gates (Fig. 2b(1)). A 170 nm-thick PECVD oxide layer was used as dielectric between CG$_1$ and floating-gate electrodes. Polyimide (PI) was then used to sandwich most of the extension of the floating gate onto the OoC sensing region. This ensured electrical insulation and mechanical robustness, while leaving the sensing electrode in contact with the environment. Fig. 2b(2) sketches the dielectric layer and first PI layer. A sputtered 300nm-thick layer of Ti was patterned to serve as CGs and FG extensions. Then a second layer of PI was spin coated and patterned to complete the insulation of the FG extensions (Fig. 2b(3)). Polydimethylsiloxane (PDMS) was mixed with its curing agent in a 10:1 ratio, degassed, spin coated and cured to serve as 20 μm-thick membrane for the OoC cell culturing/charge sensing area (Fig. 2b (4)). After sputtering a 200 nm-thick AlSi protection layer onto the PDMS (Fig. 2a(5)), the Si substrate was etched from the backside by deep reactive ion etching (DRIE) to land on the oxide layer (Fig. 2b (6)). The AlSi hard mask and residual silicon oxide were then removed by wet etching to complete the release of the PDMS membrane (front- and backside of a single sensor are sketched in Fig. 2b (7) and (8), respectively). The wafer was finally diced into 52 equal, square chips with footprint of 1 cm^2, each chip containing 4 pMOS and 4 nMOS FETs (Fig. 2(c)).

Post-processing for electrode surface structuring

The Au NP aerosols were generated by a spark discharge generator (VSP G1) and deposited by means of a
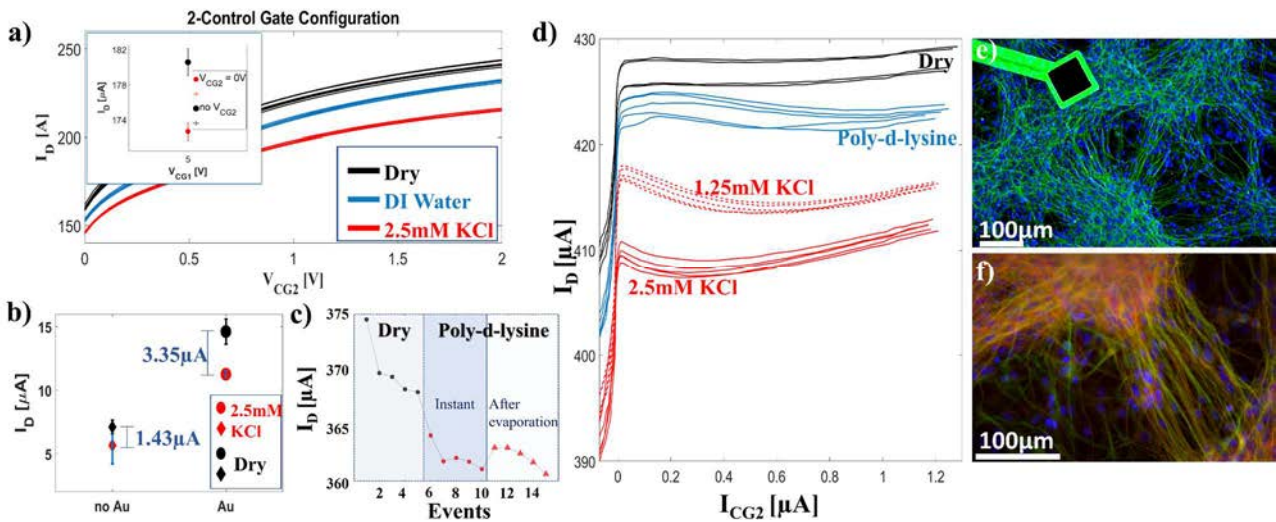
181

*Figure 3: **Characterization of nMOS-based sensors.** a) Dual-gate configuration measurements without Au decoration of the sensing electrodes. Inset shows measurements in air while applying voltage through CG_2 (red) and only using the single control-gate (black). b) Mean and standard deviation of multiple measurements on the same sensor, before and after Au decoration. The Au film increases the drain current shift for the same applied voltages (here, $V_{CG1} = 0V$ and $V_{CG2} = 2V$). c) Consecutive measurements with the same sensor in air and with poly-d-lysine. d) I_D shifts due to different liquids on Au-decorated sensor. Here, second control-gate voltages were swept (-2V to 2V) while applying constant voltage (5V) through the first control-gate. Comparison between dry (black), poly-d-lysine (blue) and KCl with different molarities (red). **Culture test on the chips with hiPSC-derived cortical neurons.** e-f) hiPSC- derived cortical neurons were stained for DAPI [e],blue], MAP2 [e], green] and synaptophysin [f], red] following 7 days of differentiation on chip.*

nanoporous material printer (NMP) prototype developed by VSParticle B.V. (Fig. 2(d)). The NMP operates at <1 mbar pressure to create an ultrasonic gas jet with tunable diameter that transfers the NPs on the substrate using their inertia [14]. The deposition process used 99.999% Au electrodes and N_2 as carrier gas, resulting in pure and clean NP film surfaces and little waste production. A 5 s deposition resulted in < 500 µm spot size.

Figs. 2(e) and 2(f) show successful damage-less completion of the Au post-processing step on the Ti sensing electrodes embedded in the 20 µm-thick PDMS membrane.

MEASUREMENTS

To characterize the sensors, a 4-probe measurement system connected to a semiconductor parameter analyzer was used to bias the FG-FETs and monitor changes in drain current I_D ensuing from charges at the sensing electrodes.

Measurements before electrode decoration

As baseline test, I_D values were recorded in air with and without applying voltage through CG_2 with the same nMOS-based sensor (inset of Fig. 3(a)). Shift in the I_D values demonstrate the electrical coupling between CG_2 and FG electrodes. After characterization in air, a 2.5mM KCl solution was introduced to the sensing area and consecutive measurements were recorded. The sensor was flushed and measurements with DI water were also recorded. The dual-gate configuration shows unique I_D characteristics for each measurement type, as evident from Fig. 3(a). We note that the absolute change in I_D value is linearly proportional to the charge concentration of the solution, whereas the negative change is attributed to the difference in dielectric constants of the solutions and to the effect of coupling capacitance between CG_2 and FG.

Measurements after electrode decoration

Effect of Au decoration. For the same sensor used previously, measurements in air and with 2.5mM KCl solution before and after Au post-processing were recorded (Fig. 3(b)). The effect of electrode decoration is evident from changes in I_D values. In addition, for the same applied voltage values, mean values of measurements after Au decoration show an up to 2.3 times increase in sensitivity.

Effect of membrane stress. After dry measurements, the Au decorated sensor was used to evaluate poly-d-lysine, a positively-charged polypeptide widely used in mammalian cell culturing [4] and stem cell research [15]. Fig. 3(c) shows shift in I_D due to reversible binding of charges in 10 µL poly-d-lysine (0.1mg/ml). Interestingly, measurements after evaporation of the solution show similar I_D values to those measured immediately after placing the solution at the sensing area. This suggests that possible membrane stress due to liquid handling did not notably affect the results, and confirms that the current shifts are primarily caused by charges bound on the electrodes.

SOT characterization: We conducted consecutive measurements of various solutions with Au-decorated FG extensions (Fig. 3(d)). First, a KCl solution (2.5mM) was introduced and measurements were recorded. The sensor was then flushed with DI water, and KCl with lower concentration (1.25mM) was introduced. Lastly, Poly-d-lysine was introduced on the sensing area. The sensor was flushed again and measurements were recorded. Changes in I_D show differences accordingly with the different charge concentrations in each solution. The low leakage current from CG_2 appears due to the reversable breakthrough of the native Ti oxide layer on top of the electrode, while applying voltage through CG_2.

182

DISCUSSION

We propose the following model to explain the increased sensitivity evidenced in the experimental results by virtue of Au electrode decoration. In the saturation regime of the transistor, the variation in the floating gate voltage ΔV_{FG} is expected to depend on the total capacitance of the device C_{TOT} and on the variation of charges in close proximity to the sensing area ΔQ [5]:

$$\Delta V_{FG} = \frac{C_{CG1}V_{CG1}}{C_{TOT}} + \frac{C_{CG2}V_{CG2}}{C_{TOT}} + \frac{Q_0}{C_{TOT}} + \frac{\Delta Q}{C_{TOT}} = \frac{\Delta Q}{C_{TOT}} \quad (1)$$

Assuming a surface charge density σ forming at the sensing electrode with surface A_S, then:

$$\Delta Q = \int_{A_S} \Delta \sigma \, ds \quad (2)$$

and I_D can be related to the floating gate voltage as:

$$\Delta I_D \cong a(\Delta V_{FG} - V_{TH})^2 \quad (3)$$

where V_{TH} is the threshold voltage and $a = \mu c_{ox} W/2L$ the FET transconductance, which depends on carrier mobility (μ), gate oxide capacitance per unit area (c_{ox}), and on width (W) and length (L) of the gate. According to (3) a change in I_D is thus in direct relation with the charge variation in close proximity to the sensing electrode. The deposition of the microscopically rough Au thin film increases the effective surface area A_S and the available sites of the sensing electrode surface.

The proposed sensor avoids the cumbersome use of an external reference electrode. While the control over the charging of the surface is not direct [11], the electrode surface enhancement method, coupled with the novel dual-gate control configuration here demonstrated, enables higher charge accumulation on the sensing electrode, thanks to the combination of electrical field between CG2 and FG and larger effective surface area.

Cell Culture & Differentiation

On chip biocompatibility and neuronal differentiation tests were conducted by culturing and differentiating human-induced pluripotent stem cell (hiPSC)-derived cortical neurons. Levels of potassium in the brain higher or lower than its threshold value might cause different disease phenotypes such as epilepsy [16] or chances of developing a headache [17]. Therefore, the ability to sense potassium from neuronal cultures *in vitro* is critically needed for brain disease modelling.

Neural Progenitor Cells (NPCs) were successfully differentiated on the chips into cortical neurons for 7 days, with staining showing mature neuron marker (MAP2/green) as well as the production of synaptic vesicle (synaptophysin/red) (Fig. 3(e-f)). Long neurite extensions are visible as well as distinct network formation, indicating that the chip is suitable for live measurements using hiPSC-derived cortical neurons.

CONCLUSION

A FET-based electrochemical sensor with enhanced sensitivity and selectivity to chemical species was integrated by a mostly CMOS-compatible fabrication process within a microelectromechanical OoC device. The dual-gate control architecture of the FETs allows higher sensitivity compared to single capacitively-coupled control-gate FETs. In addition, spark ablation was used to alter the surface morphology of the sensing electrodes with thin nanoporous Au films. This post-processing method allows fast and spatially-selective patterning over topographical substrates without the need for cumbersome and time-consuming lithography steps, and without damaging the fragile and biocompatible polymer membranes. As a result, more than doubled sensitivity was achieved, and the sensor could be used to successfully identify different SOTs, including low-concentration KCl solutions and poly-D-lysine.

Furthermore, culture tests showed that NPCs were successfully differentiated to cortical neurons on our chip, and visual inspection was possible due to the optical transparency of the culture area. These results suggest that our MEM OoC device can be employed in the near future for testing the potassium level of human brain cells (whereby normal levels of K^+ are 150 mM intracellular and 5 mM extracellular), a crucial indicator for the wellbeing and functioning of the brain [18].

REFERENCES

[1] U. Marx *et al.*, *ALTEX* 33(3), pp. 272-321, 2016.

[2] M. Mastrangeli *et al.*, *ALTEX* 36(4), p. 650-668, 2019.

[3] M. S. Thomas *et al.*, *J. Phys. Chem. Lett.* 9(6), pp. 1335-1339, 2018.

[4] B. Chen *et al., IEEE Sensors Journal*, 11(11), pp. 2906- 2910, 2011.

[5] A Spanu *et al., Scientific reports*, 5, 8807, 2015.

[6] H. Aydogmus *et. al., IEEE Sensors 2020*.

[7] P. Fromherz *et al., Science*, 252, pp. 1290-1293, 1991.

[8] S. Martinoia *et al., Biosensors and Bioelectronics*, 16(9-12), pp. 1043-1050, 2001.

[9] A. Loi *et al., Appl. Phys. Lett.* 86(10), 103512, 2005.

[10] M. Kaisti. Biosensors and Bioelectronics, 98, pp. 437-448, 2017.

[11] M. Kaisti *et al., IEEE Trans. Electron Dev.*, 62.8, pp. 2628–2635, 2015.

[12] P. Lin *et al., Adv. Mater.* 22.33, pp. 3655–3660, 2010.

[13] M. H. Park *et al., J. Phys. Chem. C* 120.9, pp. 4854–4859, 2016.

[14] Schmidt-Ott, A. (Ed.). *Spark Ablation: Building Blocks for Nanotechnology.* CRC Press, 2019.P.

[15] P. Rocheteau *et. al., Nature communications*, 6(1): 1-12, 2015.

[16] C. Simons *et. al., Nature Genetics*, 47, pp.73–77, 2015.

[17] Z. Guo, *et al., Eneuro*, 6(4), 2019.

[18] G. Florence *et. al., Communications in Nonlinear Science and Numerical Simulation,* 17(12), pp. 4700-4706, 2012.

CONTACT

*H. Aydogmus, h.aydogmus@tudelft.nl